



Ionospheric irregularities during disturbed geomagnetic conditions over Argentinian EIA region

Gilda de Lourdes González^{1,2}

Received: 19 August 2021 / Accepted: 21 December 2021 / Published online: 20 January 2022
© Akadémiai Kiadó 2022

Abstract

Ionospheric irregularities can severely degrade radio communication and navigation systems. Geomagnetic storms may affect the generation of these irregularities in a way that is not yet fully understood. To improve the forecasting of this phenomenon, we need to study the ionosphere in different regions of the world, and in particular in the equatorial ionization anomaly (EIA) where irregularities are usually more intense. This study analyses the effect of geomagnetic storms on ionospheric irregularities. We examined the occurrence of irregularities at the southern crest of the EIA in Argentina (Tucumán, 26.9°S, 294.6°E, dip latitude 15.5°S) during three intense and one moderate geomagnetic storm of different solar sources, between 2015 and 2018. We used data from an ionosonde, a Global Positioning System receiver and magnetometers. Ionogram spread-F, the F-layer bottom side ($h'F$), the critical frequency of the F2-layer (f_oF_2), the rate of TEC index and the S4 scintillation index were analysed. The data show irregularities were present as range spread-F and moderate TEC fluctuations in one storm: 27 May 2017 (a coronal mass ejection CME-driven storm occurred on local winter), and were absent in the other events. We suggest that eastward disturbance dynamo electric field and over-shielding prompt penetration electric fields may create favourable conditions for developing these irregularities, whereas westward storm time electric fields might inhibit the growth of irregularities during the other storms considered. During co-rotating interaction region CIR-driven storms, the westward disturbance dynamo electric field may be associated with the non-occurrence of irregularities.

Keywords Ionospheric irregularities · Geomagnetic storms · Equatorial ionization anomaly · Scintillation

✉ Gilda de Lourdes González
gilda.gonzalez@unsta.edu.ar

¹ Universidad Nacional de Tucumán (UNT), Tucumán, Argentina

² Universidad del Norte “Santo Tomás de Aquino” (UNSTA), Tucumán, Argentina

1 Introduction

Ionospheric irregularities are regions in the ionosphere with electron density notably different from the background. Their scale size ranges from tens of centimetres to hundreds of kilometres, and they can last from minutes to several hours. These irregularities are a major space weather issue because they can degrade navigational signals, disrupt satellite to ground communications and cause large positioning errors. Ionospheric irregularities depend on local time, season, latitude, longitude, solar, and geomagnetic activity (Abdu 2012; Madhav Haridas et al. 2018; Tsunoda 2006). At equatorial and low latitudes, the gravitational Rayleigh–Taylor instability mechanism generates the ionospheric irregularities (Balsley et al. 1972; Dungey 1956). The major driver for its generation is the vertical ExB drift (Fejer et al. 1999). A seed perturbation, e.g. gravity-waves, is also necessary for the initiation of the irregularities. A variety of techniques have been used to study this phenomenon: radar observations, ground-based Global Navigation Satellite System (GNSS), optical imaging techniques and in situ satellite measurements. Plasma density irregularities of several hundreds of meters can cause rapid fluctuations in the signal amplitude and phase in a received electromagnetic wave, called scintillation. Global Positioning System (GPS) L-band scintillations are caused by irregularities of ~400 m scale size (Briggs and Parkin 1963). Furthermore, irregularities can manifest as Total Electron Content (TEC) depletions. These are sudden reductions in TEC followed by a recovery to a level near the TEC value preceding the depletion (Valladares et al. 2004). Magdaleno et al. (2012) considered TEC depletions greater than 5 TECu (1 TECu = 10^{16} electron/m²) to be associated with plasma bubbles. In ionograms, irregularities cause backscatter signatures called spread-F; Range spread-F (RSF) if the broadening is in height and frequency spread-F (FSF) if the broadening is in the frequencies (Piggott and Rawer 1978). Night-time TEC depletions and scintillations are correlated with ionospheric irregularities at the crest of the equatorial ionization anomaly (EIA) (Dashora and Pandey 2005). Therefore, GPS derived TEC and amplitude scintillations of L-band frequencies have been used to characterize the irregularities.

The understanding of the short-term and day-to-day variabilities of the ionospheric plasma irregularities is essential to develop predictive capabilities of their occurrence. Different mechanisms drive these short-term variabilities: upward propagating atmospheric waves from the lower atmosphere (e.g. gravity waves and planetary waves), or equator-ward propagating disturbances originated during geomagnetic storms. The magnetosphere accumulates energy from the solar wind and dissipates it through geomagnetic storms that drive electrical currents and produce magnetic disturbances. At low latitudes, the ionospheric disturbances during geomagnetically active periods are mainly because of the effects of the prompt penetration electric fields (PPEFs) and the disturbance dynamo electric fields (DDEFs) (Blanc and Richmond 1980; Senior and Blanc 1984). Under southward orientation of the interplanetary magnetic field (IMF) B_z and the sudden increase in the Auroral Electrojet (AE) index—this index describes the auroral zone magnetic activity produced by enhanced ionospheric currents flowing below and within the auroral oval (Davis and Sugiura 1966)—the interplanetary electric field (IEF) is mapped to high latitudes as a dawn-dusk electric field and penetrates nearly instantaneously into low latitudes. This is called prompt penetration/under-shielding electric field and its polarity is eastward (westward) on the day-side (nightside). When B_z turns north and the AE index decreases, the associated over-shielding electric field penetrates to the low latitude ionosphere with opposite polarity of that of the under-shielding electric field (i.e. westward electric fields during the day

and eastward at night). The dynamo action of storm time winds driven by the auroral heating process produces the DDEFs. During geomagnetic storms, the energy input at high latitudes may establish a pressure gradient that affects the global wind circulations. This leads to the development of the DDEF due to plasma motion (Blanc and Richmond 1980). The DDEF has a polarity similar to that of the PPEF. It is observed several hours after the storm onset and generates long-lasting perturbations electric fields. The electric field perturbations generated by the PPEF are rapid and short-lived (2–3 h) (Fejer et al. 1979). The thermospheric winds (meridional and zonal) also play a role in the development of irregularities. During quiet times, thermospheric meridional neutral winds can uplift the F-layer at low latitudes and increase the growth rate of the Rayleigh–Taylor instability (Dao et al. 2017; Huba and Krall 2013). At post-sunset, both meridional and zonal winds may change the features of the low latitude F-layer. As it was discussed by Abdu (1997), the global changes in the thermospheric circulation due to the energy deposition at high latitudes during geomagnetic storms cause disturbances in the zonal and meridional winds. At low latitudes, these disturbance winds can modify the vertical plasma drifts and the F-layer height. Changes in the zonal wind can affect the normal development of the pre-reversal enhancement (PRE), this is the enhancement of the vertical $E \times B$ drift due to the eastward electric field at post-sunset (Rishbeth 1971). Therefore, this will influence the post-sunset irregularities generation. Whereas, the meridional (or trans-equatorial) disturbance winds may enhance the field line integrated conductivity and retard the irregularities' growth processes (Maruyama and Matuura 1984; Maruyama 1988). Then, the disturbance zonal and meridional thermospheric winds tend to inhibit the development of ionospheric irregularities (Abdu 1997). Gravity waves that induce oscillations in the F-layer height can also change the PRE and thus affect the short-term variability of the ionospheric irregularities. When the amplitude of the PRE is small, the modulation of the gravity waves is more significant and the PRE can even be suppressed (Abdu and Brum 2009).

Although several studies have been conducted, the effects of geomagnetic storms on ionospheric irregularities are not yet fully understood. Some researchers found that magnetic activity increases the occurrence of irregularities (Fejer et al. 1999). Singh et al. (2015) analysed the equatorial and low-latitude ionosphere response to an intense geomagnetic storm over the Indian sector. They showed that strong scintillation occurred at post-sunset on storm day at low latitudes. They attributed the generation of these irregularities to the enhanced TEC values due to the strong PRE. Ray et al. (2015) reported that during intense geomagnetic storms, spread-F generates within four hours of southward B_z crossing -10 nT when under-shielding condition prevails in that longitude sector for which the local time is dusk. Whereas other researchers showed that the occurrence probability of irregularities decreased during geomagnetically active periods (Lyon et al. 1960). Sahai et al. (2011) analysed the ionospheric F-region in the Latin American sector during an intense geomagnetic storm and showed that DDEFs inhibited the formation of post-sunset spread-F. Some works concluded that storms tend to trigger post-midnight spread-F (Dabas et al. 1989) and to inhibit the post-sunset ones (Aarons et al. 1980; Alex and Rastogi 1986). In the Brazilian sector, Becker-Guedes et al. (2004) reported that post-sunset spread-F was triggered during the low spread-F occurrence season, and it was inhibited during the high spread-F occurrence season. Aarons (1991) proposed that the generation or inhibition of irregularities depends on the local time in which the maximum decrease in Dst occurs. He suggested that if the minimum Dst takes place during daytime hours and before sunset (10–16 LT) then irregularities are inhibited; if minimum Dst occurs in the midnight to post-midnight (0–6 LT) then irregularities are created and if minimum Dst is observed after sunset and before midnight (18–22 LT), the F-layer height is not disturbed and the normal

pattern of the occurrence of irregularities does not change. Bolaji et al. (2019) pointed out that to study the effects of geomagnetic storms on the occurrence of irregularities, it is necessary to consider the storm timing and the local characteristics. Therefore, studies from different regions are needed to improve our understanding of the short-term behaviour of ionospheric irregularities.

In addition, it is meaningful to take heed of the solar sources of geomagnetic disturbances—coronal mass ejection (CME) or co-rotating interaction region (CIR)—since their characteristics and duration are different (Borovsky and Denton 2006). Dugassa et al. (2020) pointed out that at equatorial and low-latitudes, the response of ionospheric irregularities to a geomagnetic storm depends on its intensity and driving sources. They found the CME-driven storms led to more enhancement and suppression effects than the CIR-driven storms. They suggested that the difference in the oscillation frequency of IMF Bz in CIR and CME storms may affect the generation of PPEFs and DDEFs and, hence, the development of ionospheric irregularities.

The occurrence characteristics of ionospheric irregularities require more investigation to advance our understanding of the physical mechanisms responsible for its generation and day-to-day variability during disturbed geomagnetic conditions. Hence, improve the forecasting of the occurrence of these irregularities, especially around the EIA where they are most pronounced (Basu et al. 1988). This work aims to study the occurrence of ionospheric irregularities during geomagnetic storms at a location near the southern crest of the EIA in Argentina (Tucumán, 26.9°S, 294.6°E; magnetic latitude 15.5°S). We selected the storms based on data availability. Four events have complete data sets: 7/10/2015, 6/3/2016, 27/5/2017, and 25/8/2018. Therefore, we examined the presence of amplitude scintillation, TEC depletions and spread-F (RSF and FSF) over Tucumán during each of these four geomagnetic storms (two CME- and two CIR-driven storms).

2 Data and methodology

We used data from a GPS receiver and an ionosonde near the southern crest of the EIA in Argentina (Tucumán, 26.9°S, 294.6°E, dip latitude 15.5°S). The considered geomagnetic storms are listed in Table 1, three of them were intense and one was moderate, and they occurred in equinox and winter during the descending phase of the solar cycle 24. We classified the storms according to the Disturbed Storm Time (Dst) index (Gonzalez et al. 1999): $Dst < -100$ nT characterized an intense storm and $-100 \text{ nT} \leq Dst < -50$ nT a moderate storm. This index was obtained from the World Data Center (WDC) for Geomagnetism, Kyoto, Japan (<http://wdc.kugi.kyoto-u.ac.jp>). The value of the monthly mean solar radio flux at 10.7 cm, namely the F10.7 index, is also indicated in Table 1 to show the level of solar activity. This index is provided by Dominion Radio Astrophysical Observatory and Natural Resources Canada (<https://www.spaceweather.gc>.

Table 1 Geomagnetic storms analysed in this work, their minimum Dst value, the type of storm according to the Dst index (weak, moderate or intense), the monthly mean F10.7 (in solar flux units, sfu) and the season of occurrence

Storm day	Minimum Dst (nT)	Type of storm	Monthly mean F10.7 (sfu)	Season
7/10/2015	−124	Intense	103.3	Equinox
6/3/2016	−98	Moderate	90.6	Equinox
27/5/2017	−125	Intense	75.2	Winter
25/8/2018	−174	Intense	70.8	Winter

[ca/solarflux/sx-en.php](#)). To analyse the geospace condition during the storms, we used the North–South component (B_z) of IMF (obtained from the Advanced Composition Explorer, ACE), the zonal component (E_y) of the IEF, the Kp index (all available at <https://omniweb.gsfc.nasa.gov>), the AE index (provided by the WDC for Geomagnetism, Kyoto) and the Dst index. When the AE index was not available, we used the SuperMAG electrojet index (SME) (<https://supermag.jhuapl.edu/>). The SME index is a generalization of the AE index calculated from over 100 geomagnetic stations (12 stations are used to obtain the AE index). We got the GPS data from the Low Latitude Ionospheric Sensor Network (LISN) website (<http://lisn.igp.gob.pe>). A 25° elevation mask was used to reduce the effects of multi-path. We used the scintillation index S4 to quantify the intensity of the amplitude GPS L band scintillation (Davies 1990). S4 is defined as the normalized standard deviation of the received signal power intensity, I (Eq. 1) and it is dimensionless. $S4 > 0.5$ indicates strong scintillation activity and $0.1 < S4 \leq 0.5$ indicates weak scintillation activity.

$$S4 = \sqrt{\frac{\langle I^2 \rangle - \langle I \rangle^2}{\langle I \rangle^2}} \quad (1)$$

The vertical TEC (VTEC) was derived every 10 s using the analysis code developed by Seemala and Valladares (2011). To describe the strength of ionospheric irregularities, we used the rate of change of TEC (ROT) (Eq. 2) and the rate of TEC index (ROTI) (Eq. 3) along the signal path from each visible satellite to the receiver (Pi et al. 1997).

$$ROT = \frac{TEC_k^i - TEC_{k-1}^i}{t_k - t_{k-1}} \quad (2)$$

$$ROTI = \sqrt{\langle ROT^2 \rangle - \langle ROT \rangle^2} \quad (3)$$

where k is the time of epoch and i is the visible satellite. The sampling interval used to calculate ROT is 0.5 min, and the time window of the standard deviation of ROTI is 5 min. $ROTI < 0.25$ TECU/min indicates no TEC fluctuations, $0.25 \leq ROTI < 0.5$ indicates weak TEC fluctuations, $0.5 \leq ROTI < 1$ moderate TEC fluctuation and $ROTI \geq 1$ strong TEC fluctuations (Astafyeva et al. 2018; Ma and Maruyama 2006). This method detects irregularities with size of ~ 20 km (Nishioka et al. 2008).

The ionograms were recorded by the Vertical Incidence Pulsed Ionospheric Radar (VIPIR) and are available on the website of the Low Latitude Ionospheric Sensor Network (LISN) (<http://lisn.igp.gob.pe>). The VIPIR operates between 0.3 and 25 MHz with a sounding repetition of 5 min (Bullett 2008). Each ionogram was manually examined for the presence of spread-F. We scaled the virtual height of the F-layer bottom side ($h'F$) and the critical frequency of the F2-layer ($foF2$). To estimate the quiet-time values of $h'F$ and $foF2$ we calculated the average for the ten International Quietest Days (IQDs) and the standard deviations. Table 2 shows the ten IQDs for each month (October 2015, March 2016, May 2017 and August 2018), the maximum Kp and minimum Dst values for each group of days. The IQDs are defined according to the geomagnetic Kp index, the GFZ German Research Centre for Geosciences use three criteria to select the IQDs for each month: the sum of the eight Kp values, the sum of squares of the eight Kp values and the maximum of the eight Kp values. The days are ordered and numbered according to these criteria, for each day the mean of these three numbers is a measure

Table 2 The ten International Quietest Days (IQDs) for the months with storms, the maximum Kp and minimum Dst values for each group of days

Month	Ten Quietest days	Maximum Kp	Minimum Dst (nT)
October 2015	26, 28, 27, 19, 29, 22, 23, 31, 16 and 25	2.7	− 1
March 2016	26, 13, 5, 4, 25, 22, 24, 31, 9 and 3	2.3	− 4
May 2017	26, 25, 6, 24, 13, 31, 6, 2, 5 and 1	2.3	− 3
August 2018	6, 14, 10, 13, 23, 30, 9, 5, 8 and 31	2.3	− 27

of its relative geomagnetic activity within this month (Matzka et al. 2021). IQDs can be obtained at <https://www.gfz-potsdam.de/en/kp-index/>.

We used the ΔH parameter to study the occurrence of penetration electric fields. ΔH is the difference in the magnitudes of the horizontal geomagnetic field component (H) between a magnetometer placed on the magnetic equator (Jicamarca, dip latitude 0.4°N) and one displaced $6^\circ\text{--}9^\circ$ away, outside the equatorial electrojet (EEJ) influence (Piura, dip latitude 6.8°N). ΔH is related to the EEJ strength and provide an approximation of the zonal electric field during daytime (De Siqueira Negreti et al. 2017; Wei et al. 2015), this is between 11:00 and 23:00 UT in the Peruvian sector. The magnetometer data can be downloaded from the LISN website.

3 Results

3.1 Storm of 7 October 2015

An intense geomagnetic storm ($\text{Dst}_{\min} = -124\text{nT}$, $\text{Kp} = 7$) occurred in the early hours of 7 October 2015 (equinox) due to a CIR. This is a boundary zone between slow- and fast-moving solar wind streams. The Dst index showed a two-step response (Fig. 1); it decreased to -93 nT at 9 UT (6 LT) then it recovered and decreased again to its minimum value at 22 UT (19 LT). This is a two-phase geomagnetic storm: two main phases and two recovery phases. The highest Kp value ($\text{Kp} = 7$) was seen at 18 UT (15 LT) on 7 October, AE was highly variable with a peak of 1227 nT at 18 UT (15 LT), a similar irregular behaviour was observed in IMF Bz, it oscillated rapidly between north and south. Whereas Ey (that is proportional to $-V_{\text{sw}} \times B_z$ where V_{sw} is the solar wind speed) also showed oscillations but remained eastward most of the time.

The RSF occurrence rate (number of days with RSF divided by the number of days with data available in a month) during October 2015 was 70%, the FSF occurrence was 20% and the plasma bubble occurrence, detected as TEC depletion greater than 5 TECu (Magdaleno et al. 2012), was 16% (Fig. 2). However, no TEC depletions were observed during the period of the storm, and S4 was always below 0.2 (Fig. 3). We did not observe spread-F despite h'F is higher than the values for quiet-time between $\sim 0\text{--}10\text{ UT}$ ($21\text{--}7\text{ LT}$) on 7 October (Fig. 4). During the period of the storm, foF2 were close to those of quiet days except on 7 October at $0\text{--}6\text{ UT}$ ($21\text{--}3\text{ LT}$) when foF2 was lower during disturbed days than during quiet days, this decreased in foF2 is called negative ionospheric storm. There was an irregular behaviour in ΔH (Fig. 5) on 7 October between 13 and 21 UT ($10\text{--}18\text{ LT}$).

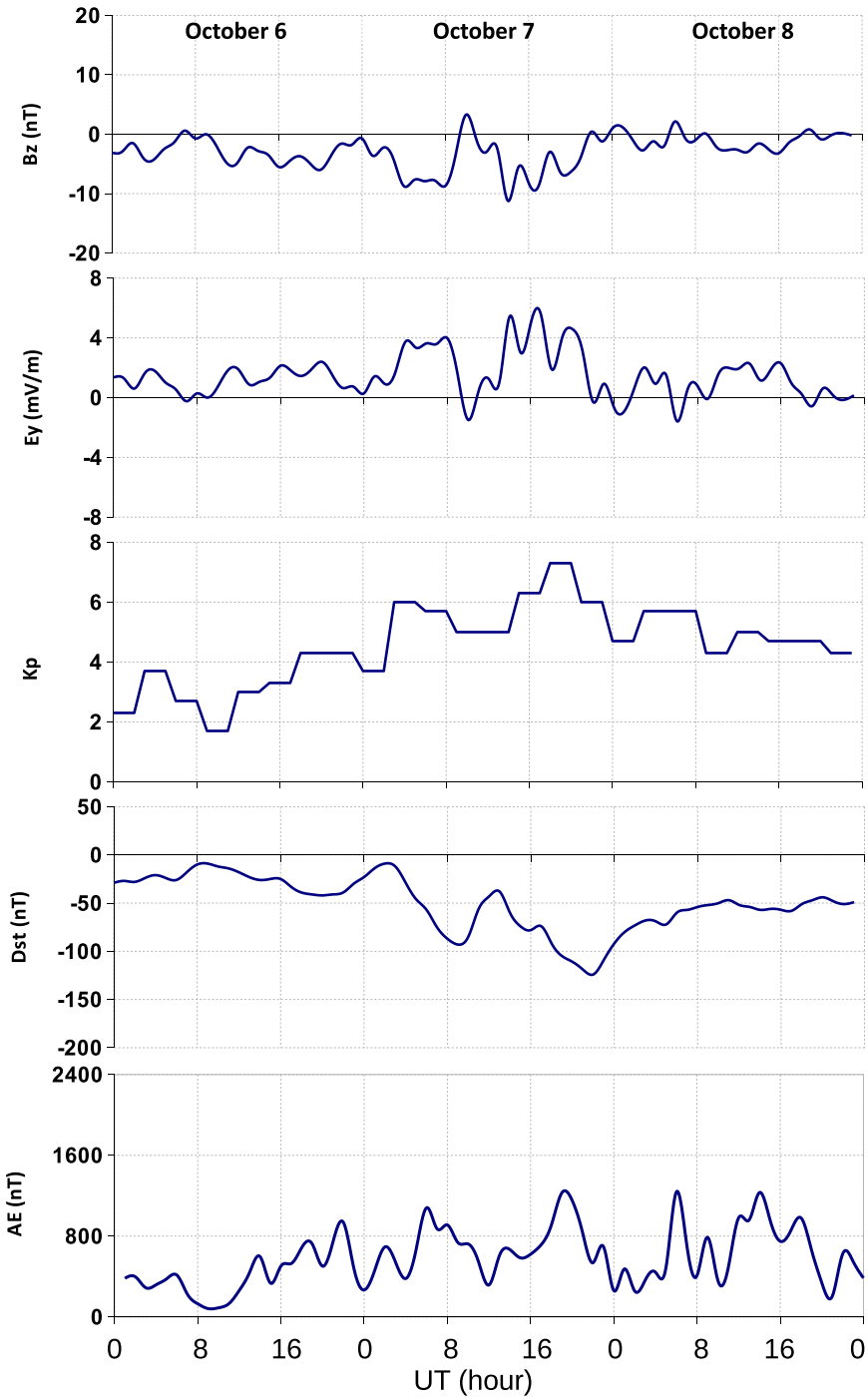


Fig. 1 Bz, Ey, Kp, Dst and AE during 6–8 October 2015

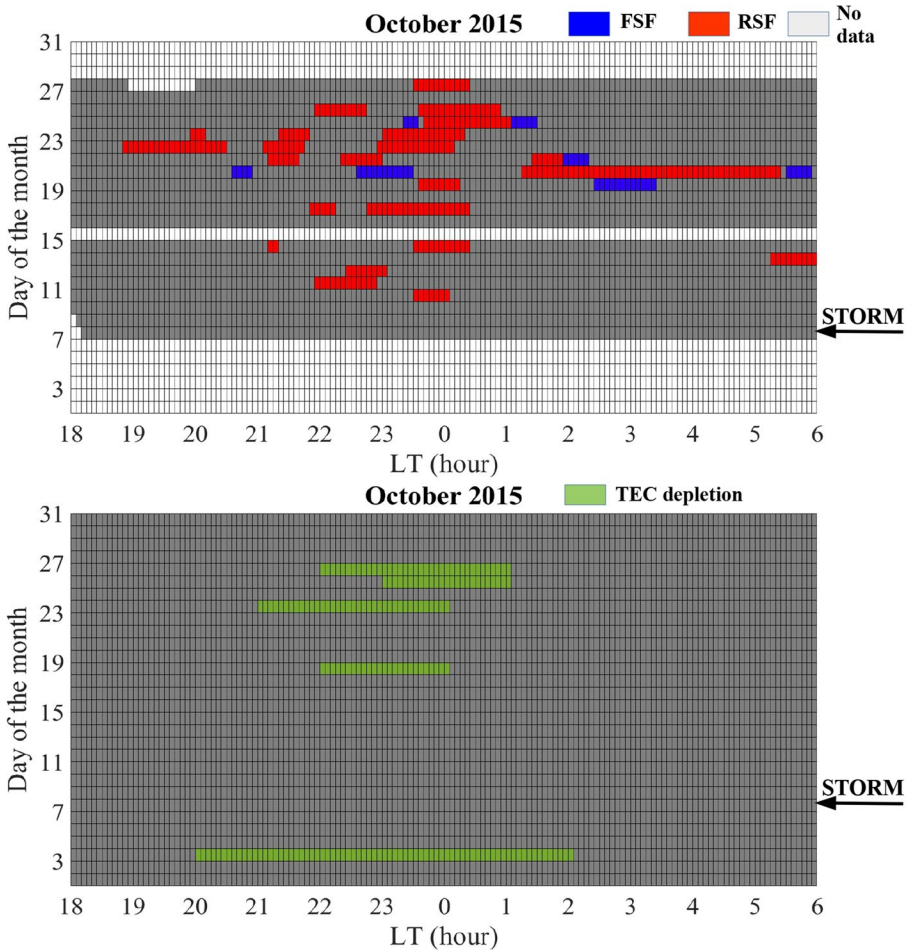


Fig. 2 Top panel, range spread-F (RSF) occurrence (red) and frequency spread-F (FSF) occurrence (blue) at Tucumán during October 2015. White indicates data gaps. Bottom panel, strong TEC depletions occurrence (green) during October 2015. (Color figure online)

This may be related to the oscillations in IMF Bz, a characteristic of CIR-driven storms. ΔH showed negative values around 17 UT (14 LT) that could be a signature of the presence of a westward electric field.

3.2 Storm of 6 March 2016

A moderate geomagnetic storm occurred on 6 March 2016 (equinox) when a CIR hit the Earth's magnetic field (Fig. 6). The minimum Dst (-98 nT) and the maximum Kp index (6) were observed at 21 UT (18 LT). AE showed its highest value (1177 nT) at 17 UT (14 LT), decreased and then increased again to a second peak (770 nT) at 22 UT (19 LT) and it was highly variable during the rest of the day and on the next day. Ey has an irregular behaviour mainly with positive values with peaks of 4.8 mV/m at 18 UT (15 LT),

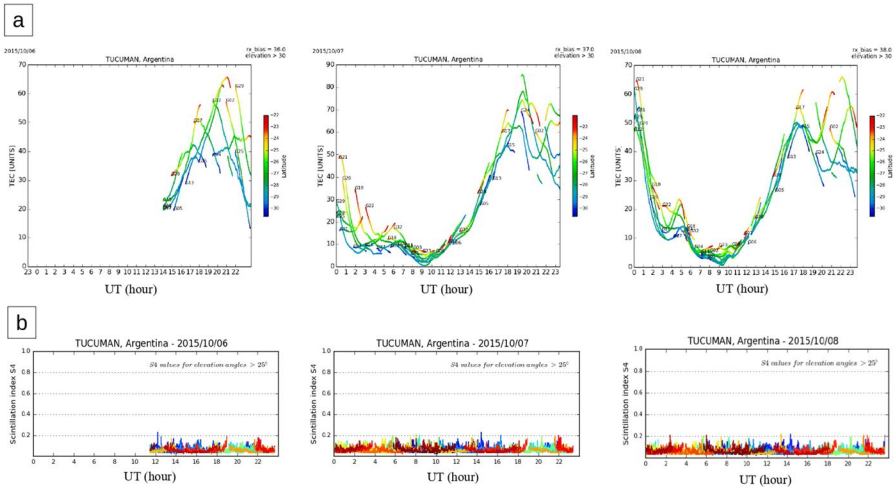


Fig. 3 **a** TEC for different satellites at Tucumán on 6, 7 and 8 October 2015. **b** S4 index for different satellites on 6, 7 and 8 October 2015. Different colours indicate different satellites

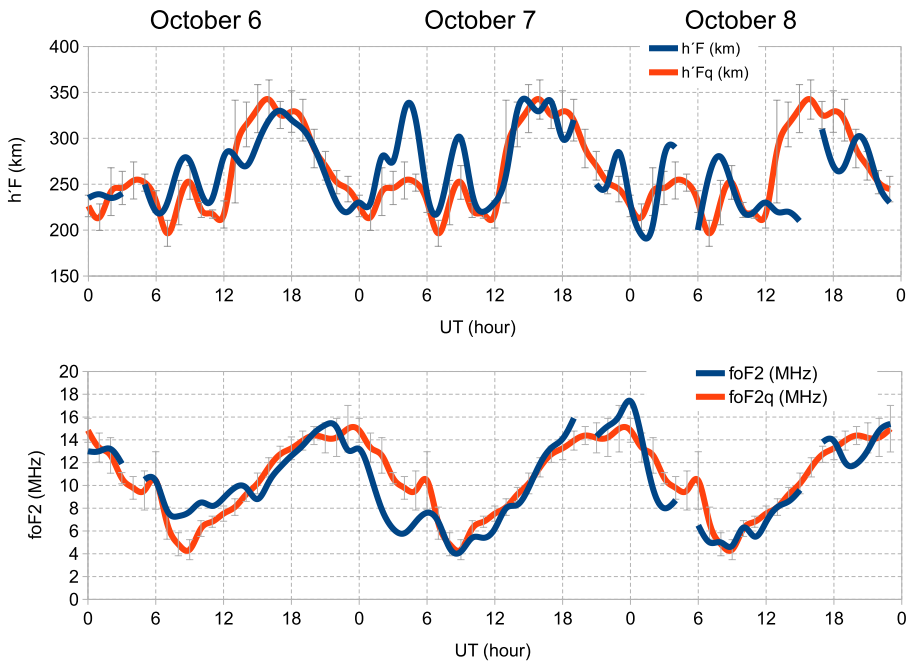


Fig. 4 $h'F$ and $foF2$ at Tucumán during 6–8 October 2015. The grey lines are ± 1 standard deviation of the average quiet day's value

4.7 mV/m at 16 UT (13 LT) and 4.1 mV/m at 21 UT (18 LT) on 6 March. B_z turned south at ~ 8 UT (5 LT), and from 16 UT (12 LT) exhibited an oscillatory behaviour between north and south. The oscillations diminished after ~ 8 UT (5 LT) on 7 March. During each southward turning, the eastward electric field increased.

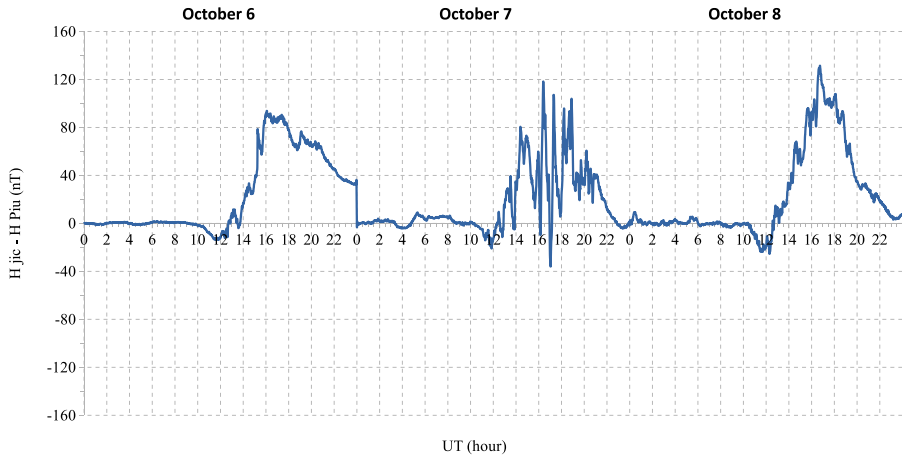


Fig. 5 Difference between horizontal geomagnetic field components (H) at Jicamarca and Piura, Peru, during 6–8 October 2015

In March 2016, 48% of the days showed RSF, 30.4% showed FSF (Fig. 7) and one day showed strong TEC depletion (not shown here) before the start of the storm: 6 March between 1 and 3 UT (22–0 LT) in coincidence with strong scintillation activity. During the period of the storm, the S4 index was usually lower than 0.2 (Fig. 8a) and no TEC fluctuation neither spread-F were observed. As an example, Fig. 8c shows ROTI values for some satellites on 6 and 7 March and Fig. 8d depicts the satellite tracks. Usually, h'F was close to its quiet-time reference value during the period of the storm (Fig. 9), except for 6 March at 19 UT to 7 March at 3 UT and 7 March between 7 and 11 UT when storm-time h'F was higher than quiet-time h'F, on 8 March between 14 and 21 UT h'F was lower than during quiet-times. Finally, foF2 during disturbed days was similar to the quiet values, except for a negative ionospheric storm phase observed on 7 March from 18 to 24 UT.

ΔH was highly variable during the period of the storm (Fig. 10), with negative values on 6 March around 17:30–18:20, 18:30–19:30 and 19:40–20:10 UT (14:30–15:20 LT, 15:30–16:30 LT and 16:40–17:10 LT), this may be related to westward electric fields. Whereas, positive values were observed at 18:20–18:30 UT, 19:30–19:40 and after 20:10 UT. The period 17–21 UT on 6 March corresponds to the main phase of the storm when IMF Bz oscillated from north to south and vice versa and AE showed periods of increase and decrease. This may explain the irregular behaviour observed in ΔH .

3.3 Storm of 27 May 2017

An intense geomagnetic storm occurred on 27 May 2017 (local winter) when an interplanetary CME hit Earth's magnetic field at 15:34 UT (12:34 LT), (the time of sudden storm commencement, SSC, was obtained from the International Service on Rapid Magnetic Variations of the Ebre Observatory, <http://www.obsebre.es/en/rapid>). The minimum Dst (–125 nT) was seen on 28 May at 7 UT (4 LT) and the highest Kp (7) occurred at 3 UT (0 LT) (Fig. 11). Bz presented a strong southward excursion with a peak of –20 nT whereas Ey increased during the storm main phase and reached 7.7 mV/m on 28 May at 0 UT (21 LT). AE showed three peaks, 949 nT at 23 UT (20 LT) on 27 May, 1163 nT at ~2 UT (23 LT) and 1270 nT at ~5 UT (2 LT) on 28 May. A second enhancement of the geomagnetic

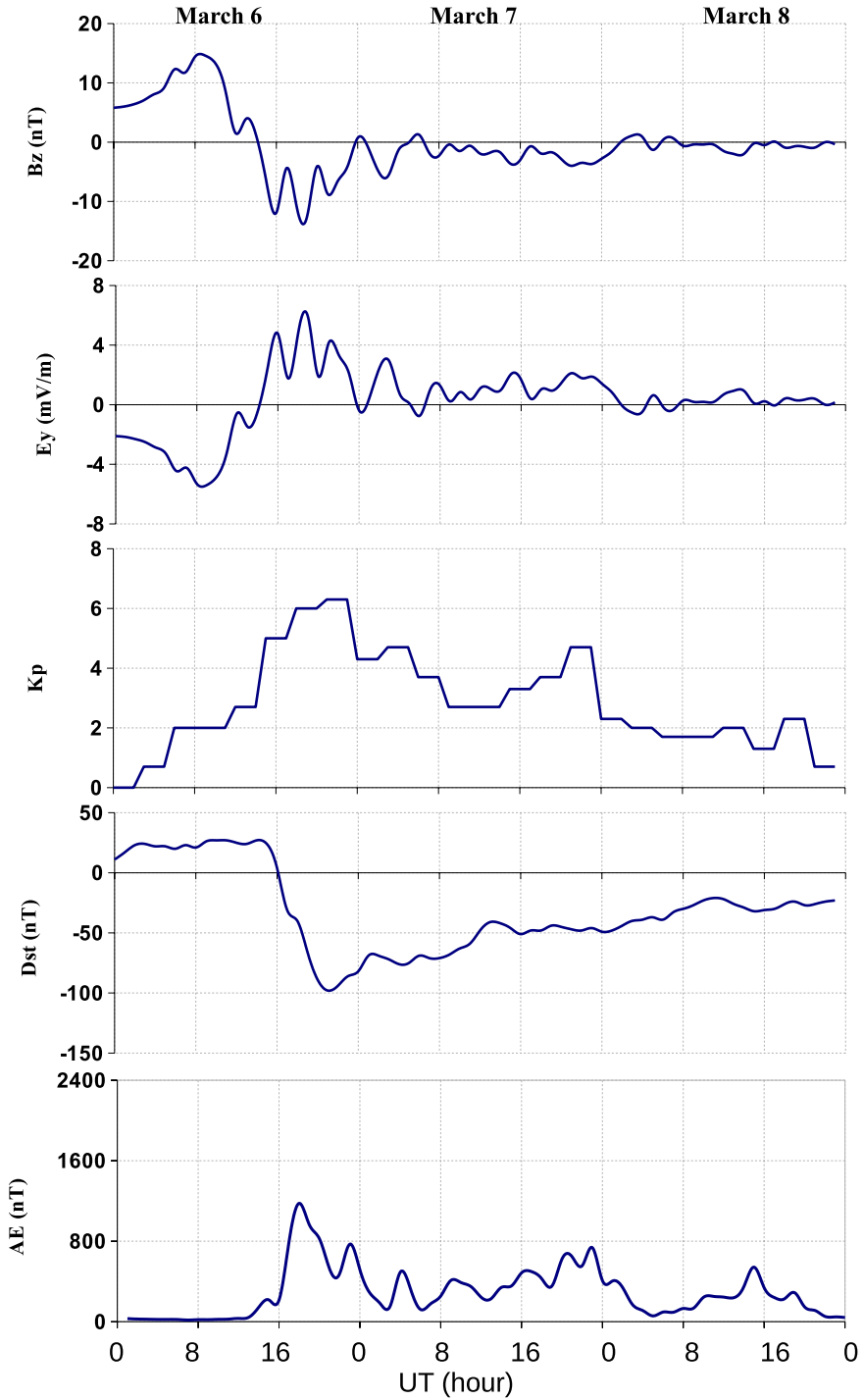


Fig. 6 Bz, Ey, Kp, Dst and AE during 6–8 March 2016. (Color figure online)

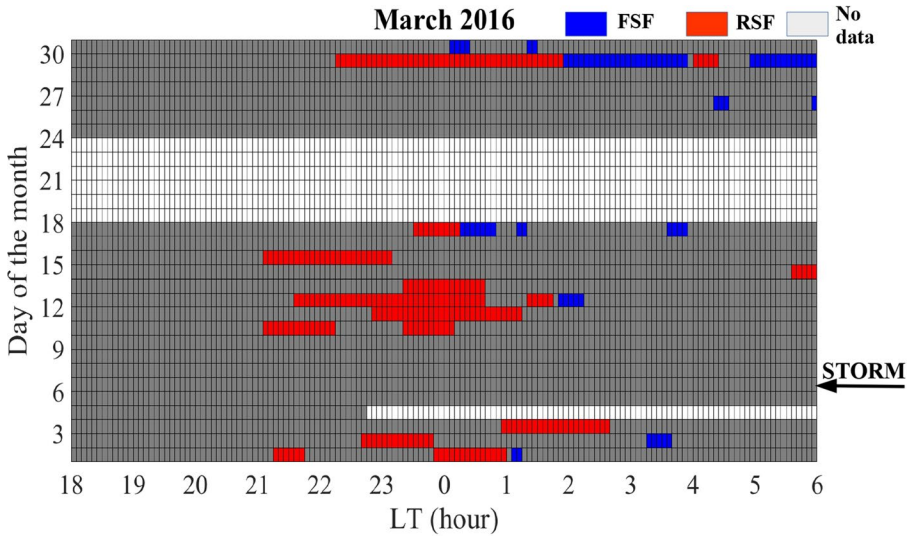


Fig. 7 Range spread-F (RSF) occurrence (red) and frequency spread-F (FSF) occurrence (blue) at Tucumán during March 2016. White indicates data gaps. (Color figure online)

activity occurred on 29 May at ~13 UT (10 LT): B_z reached -12 nT, $E_y = 4.5$ mV/m, $K_p = 4$ and one hour later AE was 839 nT.

During the period of the storm, we observed weak L band scintillation activity (Fig. 12a). TEC depletions were seen during the main phase of the storm, on 28 May around 1–5:30 UT (22–2:30 LT) (Fig. 12c) but TEC depletion greater than 5 TECu were only present in one day of the month: May 4 (not shown here). According to the ROTI values, moderate and weak TEC fluctuations were present during the main phase of the storm on 28 May around 2 UT. Figure 12d depicts some examples for PRN 13, 15, 17 and 24 and Fig. 12e shows their trajectories. The RSF occurrence rate was 64.5% in May 2017 and, during the main phase of the storm, RSF was present for several hours: on 28 May from 00:43 to 7:33 UT (27 May, 21:43–28 May, 4:33 LT). Figure 12b shows an example of an ionogram with RSF recorded on 28 May, and Fig. 13 depicts the RSF and FSF occurrence during the entire month. An increase in $h'F$ was seen on 28 May at 0–6 UT (Fig. 14), when it was higher than the quiet-time levels. Unfortunately, we were unable to obtain the height values on 28 May between 6 and 10 UT because of the presence of spread-F in the ionograms. During 27 and 29 May, storm-time $h'F$ was similar to the quiet-time $h'F$. The f_oF_2 was usually close to the quiet-time levels, except on 28 May at ~14–20 UT, when a positive ionospheric storm (increase in f_oF_2) was observed. ΔH showed positive values during the period of the storm considered, whereas it was negative on 29 May at ~11:30–14 UT (8:30–11 LT) when a substorm was observed, negative values in ΔH may be the effect of westward electric fields (Fig. 15).

3.4 Storm of 25 August 2018

On 25 August 2018 (local winter), an interplanetary CME hit the Earth's magnetic field and triggered an intense geomagnetic storm. The source of this CME was probably a

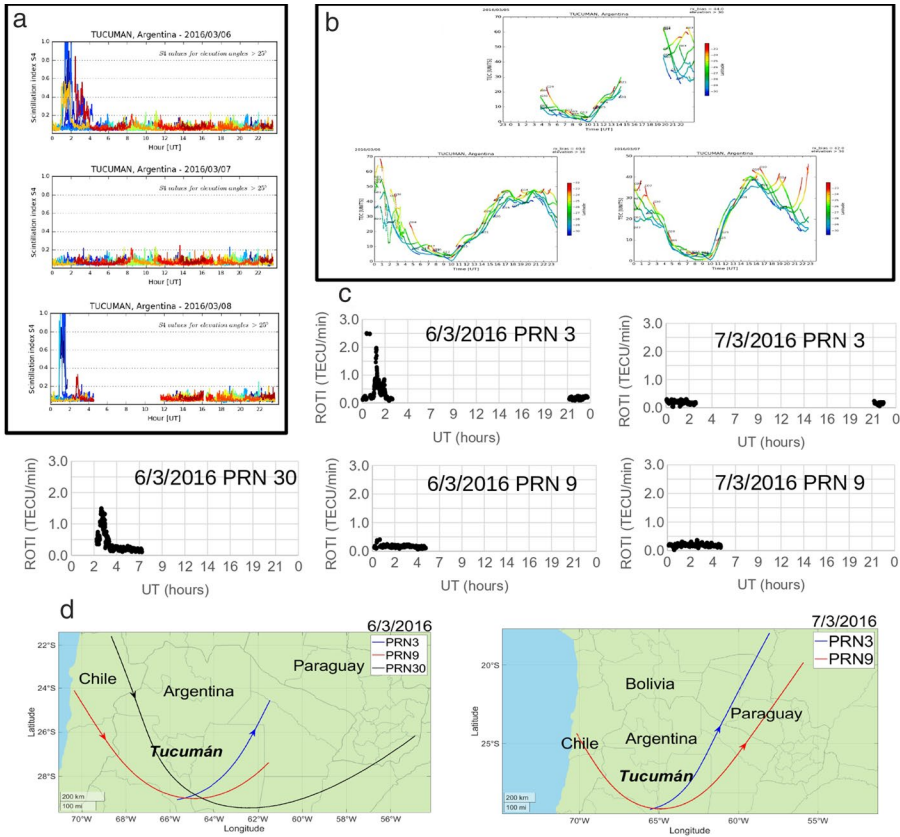


Fig. 8 **a** S4 index at Tucumán during 6–8 March 2016. Different colours indicate different satellites. **b** TEC for different satellites at Tucumán during 6–7 March 2016. **c** ROTI for PRN 3, 9 and 30 on 6 and 7 March 2016. **d** Trajectories of PRN 3, 9 and 30 on 6 and 7 March 2016 for the periods considered in the plots shown in c. (Color figure online)

filament eruption observed on 20 August (Piersanti et al. 2020). The Dst reached a minimum value of -174nT and K_p a maximum of 7 at ~ 7 UT (4 LT) on 26 August (Fig. 16). B_z flipped southward on 25 August at ~ 16 UT (13 LT) and showed an oscillatory behaviour on 26 August at 8–20 UT (5–17 LT). E_y increased from 25 August at 14 UT (11 LT) and peaked at 5 UT (2 LT), like B_z , E_y also presented an irregular behaviour after 8 UT on 26 August, with mostly positive values. There were no data available for the AE index during the period of the storm, so we decided to use the SME index to evaluate the auroral zone magnetic activity. SME increased from 25 August at around 17 UT (14 LT) and its highest value was 1565 nT at ~ 3 UT (~ 0 LT) on 26 August. Then, it irregularly decreased to quiet values and increased again after 0 UT on 27 August (22 LT on 26 August).

During the period of the storm, S4 was usually lower than 0.2 and ROTI was lower than 0.5, this means weak L band scintillation and weak TEC fluctuation were present. Figure 17 depicts the S4 index and, as an example, the ROTI for PRN 26 during 25–27 August 2018. There were no ionosonde data for most of August 2018, so we did not calculate the spread-F occurrence rate for this month, however previous researchers have found that in winter months during low solar activity—such as August 2018—spread-F occurrence

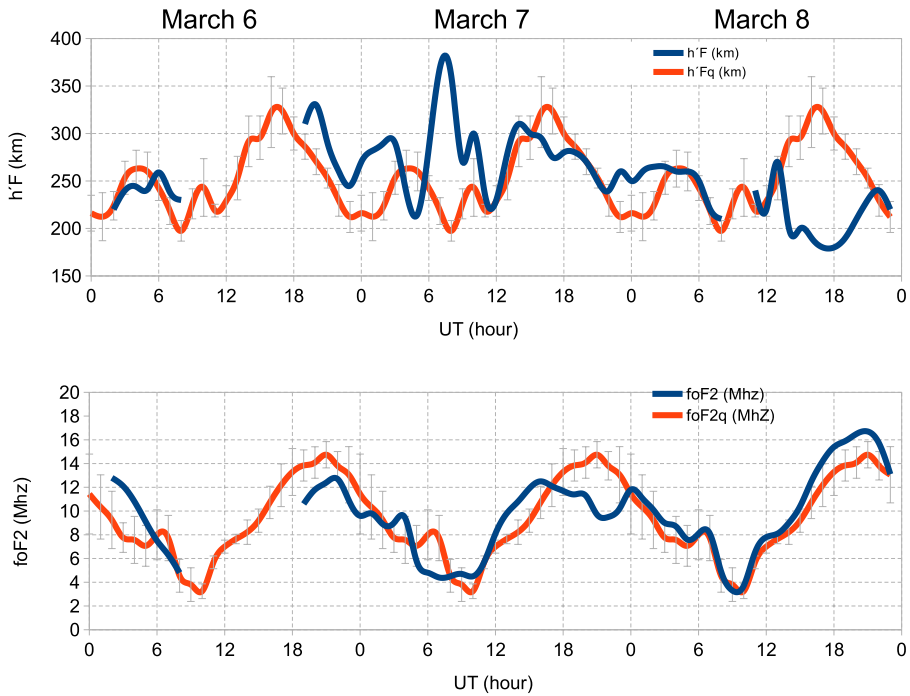


Fig. 9 $h'F$ (top) and $foF2$ (bottom) for Tucumán during 6–8 March 2016. The grey lines are ± 1 standard deviation of the average quiet day's value

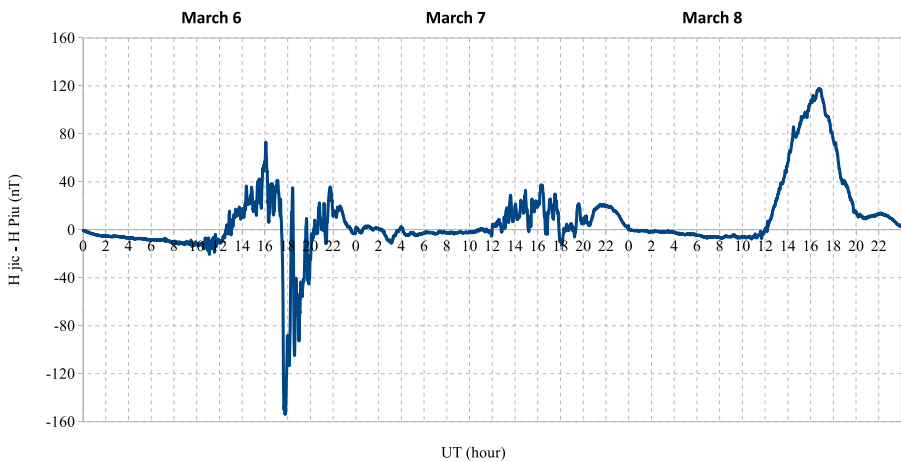


Fig. 10 Difference between horizontal geomagnetic field components (H) at Jicamarca and Piura, Peru, during 6–8 March 2016

is high at the southern crest of the EIA (Candido et al. 2011). But, during the days of the storm, the ionograms did not show spread-F. The disturbed $h'F$ values were usually similar to the quiet-time values (Fig. 18) but on 26 August at ~ 20 UT (~ 17 LT) $h'F$ was

higher during the storm than during quiet days. Whereas, a positive ionospheric storm was observed on 26 August at 0–6 UT (21–3 LT), at 12–18 UT (9–15 LT) and on 27 August at 12–19 UT (9–16 LT). ΔH (Fig. 19) was negative on 26 August at 11–15 UT (8–12 LT) and 15:30–18:30 UT (12:30–15:30 LT), during part of the main phase and the recovery phase of the storm. $\Delta H < 0$ also during 25 August at 11–13 UT and on 27 August around 12 UT. ΔH was positive on 26 August at ~19–23 UT (~16–20 LT), during the recovery phase.

4 Discussion

Only one of the four geomagnetic storms showed ionospheric irregularities (spread-F in ionograms, TEC depletions and GPS L band scintillation): 27 May 2017. This was an intense storm driven by a CME. It occurred in local winter during low solar activity (mean $F10.7 = 75.2$ sfu). RSF, moderate TEC fluctuation and weak GPS L band scintillation were seen during the storm's main phase. The RSF started at ~22 LT on 27 May and lasted until ~4 LT on 28 May. Whereas, the TEC fluctuation vanished around 2 LT. During this period, B_z was turning north, E_y was decreasing and AE was increasing irregularly. These irregularities may be related to an eastward DDEF that might be acting since the irregularities were seen several hours after the storm onset. Another possibility is the effect of an over-shielding eastward electric field that reached low latitudes, associated with the B_z turning north at this time. ΔH is used to assess the occurrence of penetration electric fields during the daytime, due to higher Cowling conductivity during the day than at night. However, several researchers reported PPEF signatures in ΔH on the nightside (Fejer et al. 2007; Galav et al. 2011). Moreover, Wei et al. (2013) concluded that nightside ΔH can sometimes manifest a PPEF in the midnight-dawn sector (00–05 LT). We observed that on 28 May, ΔH increased between 2–8 UT (23–5 LT), this may be associated with an eastward penetration electric field.

During this storm, we observed RSF, but the amplitude scintillation was weak. The ionospheric irregularities detected by the ionosonde and the GPS receiver are of different sizes; the amplitude scintillation is caused by irregularities of few hundreds of meters of scale-size whereas, the ionosonde can detect larger-scale irregularities (> 1 km) (de Paula et al. 2007 and references therein). Therefore, the irregularities present on this day may be larger than those necessary for scintillation to occur.

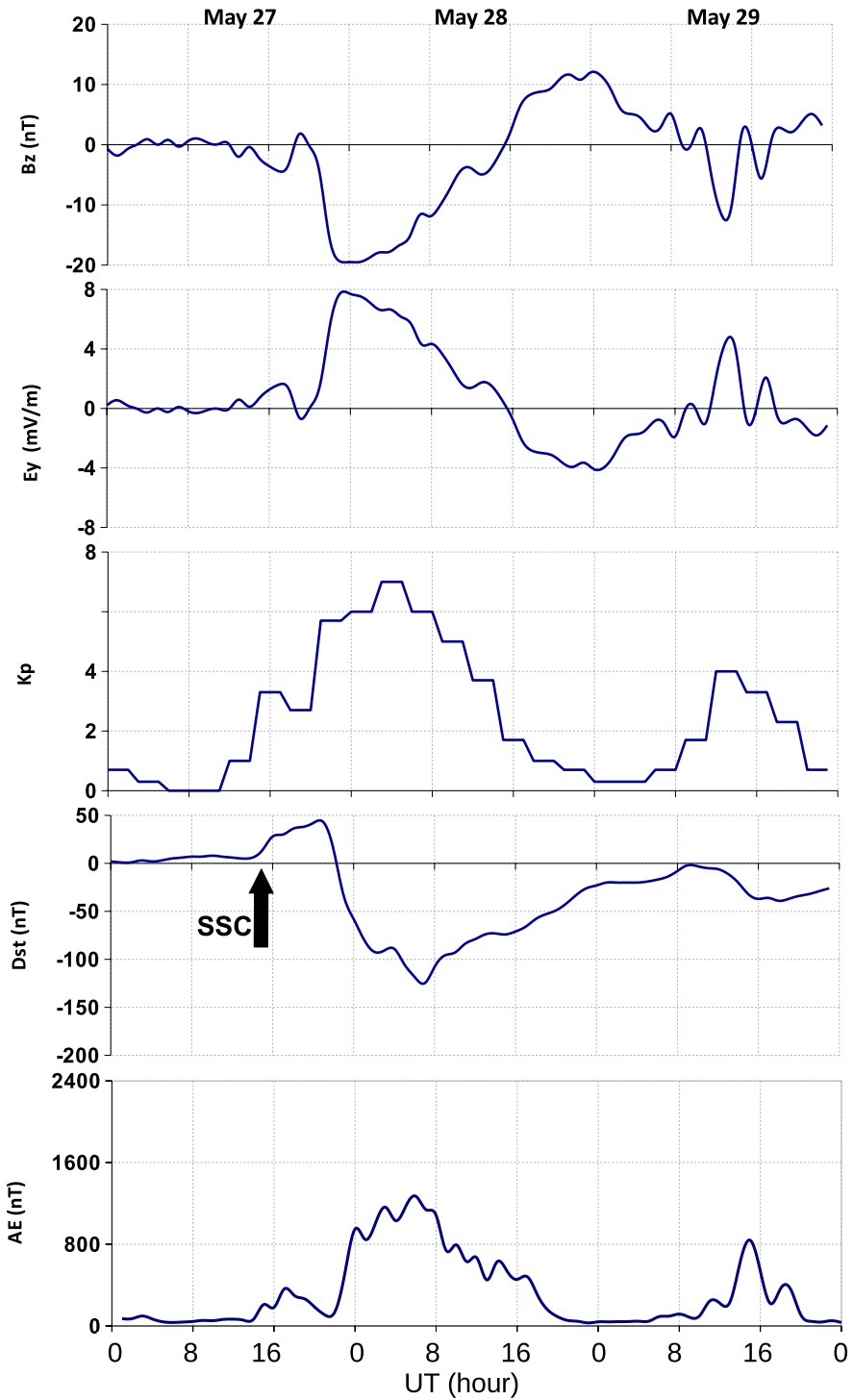
Our observations for the May storm suggest eastward storm time electric fields (PPEF and/or DDEF) may induce disturbance upward $E \times B$ drifts that rise the F region to heights of lower ion-neutral collision frequency and lower recombination rate. An increase in the $h'F$ values was observed during the main phase of the storm. This could enhance the growth rate of the gravitational Rayleigh–Taylor instability mechanism and help create favourable conditions for irregularities to develop (if a seed perturbation is present) (Dungey 1956; Fejer et al. 1999). The results are consistent with the studies carried out by Abdu et al. (2012). They concluded that post-midnight spread F can develop from over-shielding electric fields during two moderate geomagnetic storms at low latitudes in Brazil. Also in Brazil, Saha et al. (2007) reported plasma bubbles during the recovery phase of an intense geomagnetic storm in winter. For the other storms under consideration, PPEFs and/or DDEFs of westward polarity may cause a downward drift of the F-region plasma and might inhibit the formation of irregularities. Possible signatures of these westward electric fields can be observed in ΔH on 6 March between 17:30 and 20 UT (14:30–17 LT) and on

Fig. 11 Bz, Ey, Kp, Dst and AE during 27–29 May 2017. The arrow indicates the sudden storm commencement (SSC) ▶

26 August between 11 and 18:30 UT (8–15:30 LT). It is important to note that on 6 March between 19 and 20 UT, when ΔH is negative, h'F is higher than during quiet-time. At low latitudes in Brazil, de Paula et al. (2019) reported that ionogram spread-F, GPS and VHF amplitude scintillations were completely inhibited during a geomagnetic storm in September 2017. They suggested westward DDEFs caused a strong counter-electrojet (negative ΔH values) and a downward movement of the F-layer height, and therefore suppressed the formation of irregularities. In the American sector, de Abreu et al. (2017) showed that ionospheric irregularities were not affected by the intense geomagnetic storm on 1–3 June 2013. Dugassa et al. (2020) reported that during the solar minimum period 2007 to 2009, there were no significant effects of geomagnetic storms in the occurrence of ionospheric irregularities over low-latitudes in Africa. Previous studies observed similar behaviour in different longitudes e.g. Abdu et al. (2006), Amaechi et al. (2018), Ngwira et al. (2013). In the present work, we may attribute the absence of ionospheric irregularities in three of the four storms examined to the effect of westward DDEFs and/or westward PPEFs. An over-shielding (under-shielding) electric field associated with the northward (southward) orientation of Bz acting during post-sunset (post-midnight) hours may suppress the generation of ionospheric irregularities at the southern crest of the EIA. Irregularities usually occur after large and consistent southward excursions in Bz during post-sunset (Martinis et al. 2005), for the CIR-driven storms (October and March storms) and during the recovery phase of the August storm, the oscillatory behaviour—several short-lived southward and northward turnings—in Bz may create several under-shielding and over-shielding electric fields with opposite polarity. Therefore, the effect of the PPEFs may not be significant. We suggest the DDEF could be the primary cause of the inhibition of irregularities. However, other parameters might affect the development of irregularities during disturbed periods at low latitudes, e.g. gravity waves or travelling ionospheric disturbances (TIDs) due to storm time Joule heating in the auroral zone (Abdu et al. 2012; Deng et al. 2021). The role of these phenomena can be examined in further studies, e.g. using meridional ionosonde data.

The minimum Dst during the May storm occurred in the post-midnight period and, according to Aarons (1991) the F-layer height should rise and create irregularities. Our observations agree with this hypothesis. However, the August storm also presented the minimum Dst at post-midnight, but we did not detect irregularities. During the October and March storms, the minimum Dst took place after sunset, Aarons (1991) suggests the storm has no significant effect and irregularities may form as on a quiet night, nevertheless, we did not see post-sunset irregularities that were present in several quiet days in October and March. Shang et al. (2008) analysed the effect of strong geomagnetic storms on L-band ionospheric scintillation over the eastern Asia equatorial region, they showed that for CME-driven storms, when the maximum negative excursion of Dst occurs after 03 LT to the early morning hours, no scintillation was observed in the latter half of the night. Our results for the May storm and for the August storm (both driven by CMEs) agree with this conclusion. For these events, the minimum Dst took place at 4 and 3 LT respectively, and we did not see irregularities during the rest of the night. For the May storm, spread-F vanished at ~4 LT, whereas for the August storm, no irregularities were detected.

On 6 October at 21–7 LT and on 7 March at 4–8 LT the F-layer rise to higher values than during quiet time, but irregularities were not detected, this may imply that other



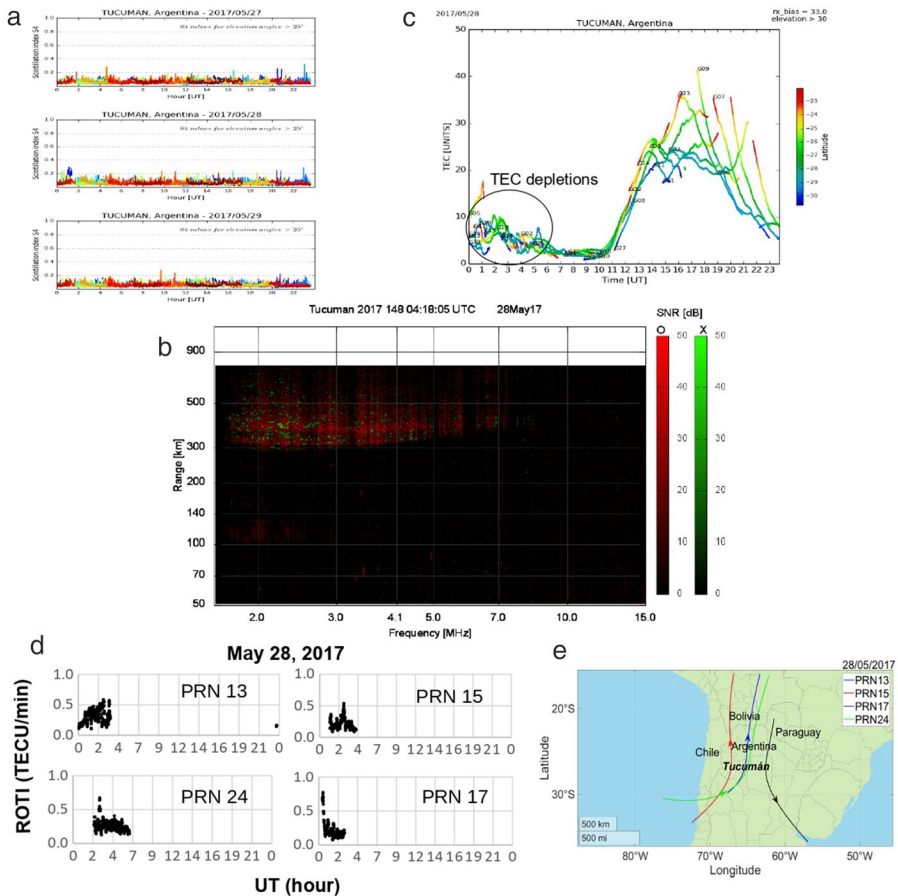


Fig. 12 **a** S4 index at Tucumán during 27–29 May 2017. Different colours indicate different satellites. **b** Example of RSF observed in ionograms on 28 May 2017 at Tucumán. **c** TEC at Tucumán on 28 May. The circle indicates TEC depletion. **d** ROTI for PRN 13, 15, 24 and 17 on 28 May 2017. **e** Trajectories of PRN 13, 15, 17 and 24 on 28 May 2017 for the periods considered in the plots shown in (d). (Color figure online)

processes could inhibit the development of the irregularities at this time. Moreover, we observed negative ionospheric storms on 7 October at 0–6 UT (21–3 LT) and on 7 March from 18 to 24 UT (15–21 LT). At low latitudes, changes in the F-layer height can be caused by the disturbance thermospheric meridional winds generated in the auroral zone that travel to the equatorial region (Sahai et al. 2011), F-layer height increases in the upwind hemisphere whereas it decreases in the downwind hemisphere. Shang et al. (2008) suggested that the disturbance of neutral winds might be responsible for the suppression of scintillation. This conforms to previous researchers (Maruyama 1988; Abdu 1997) who pointed out that the meridional disturbance winds that control the flux tube-integrated conductivity and the F-layer bottom side gradient may inhibit or slow down the development of ionospheric irregularities by modifying its growth rate. Also, trans-equatorial winds can

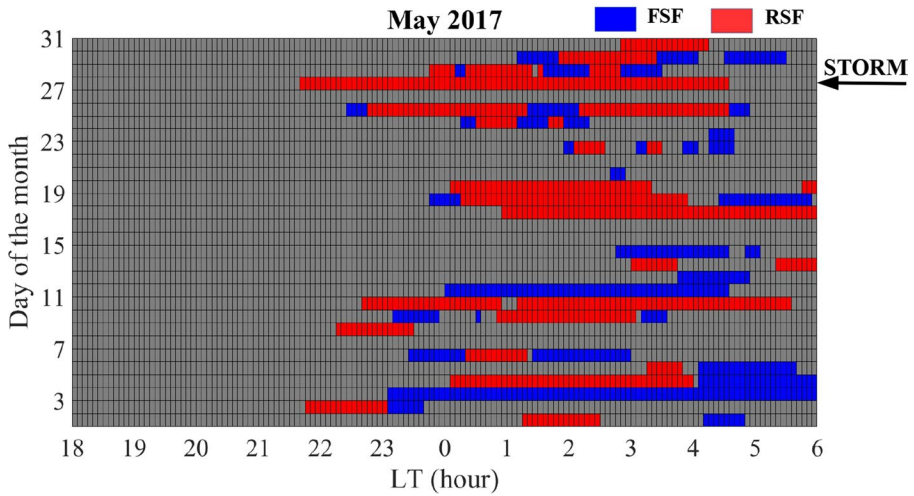


Fig. 13 Range spread-F (RSF) occurrence (red) and frequency spread-F (FSF) occurrence (blue) at Tucumán during May 2017. (Color figure online)

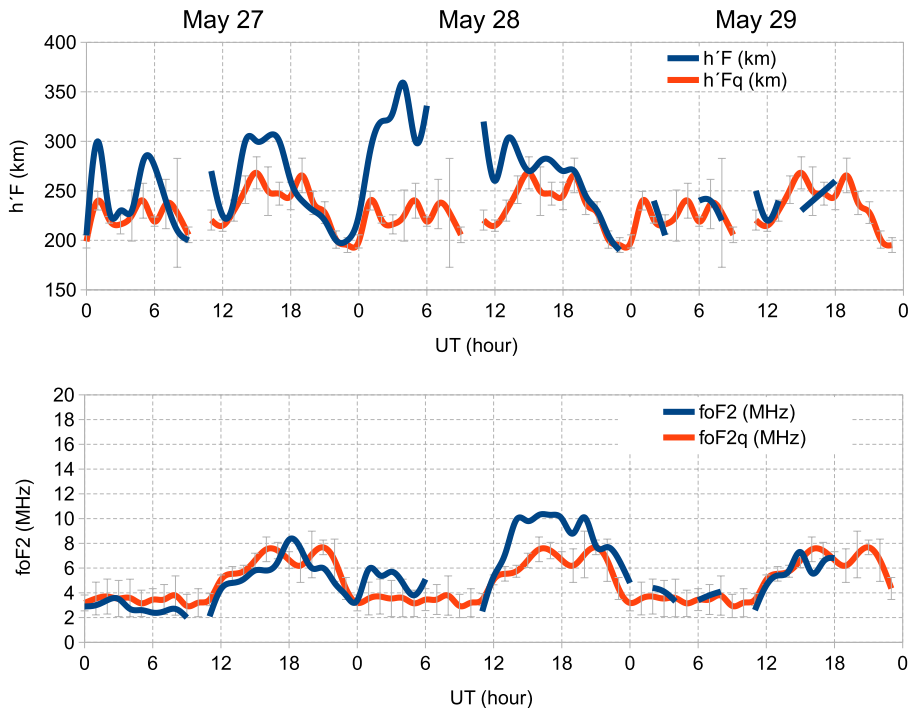


Fig. 14 $h'F$ (top) and $foF2$ (bottom) for Tucumán during 27–29 May 2017. The grey lines are ± 1 standard deviation of the average quiet day's value

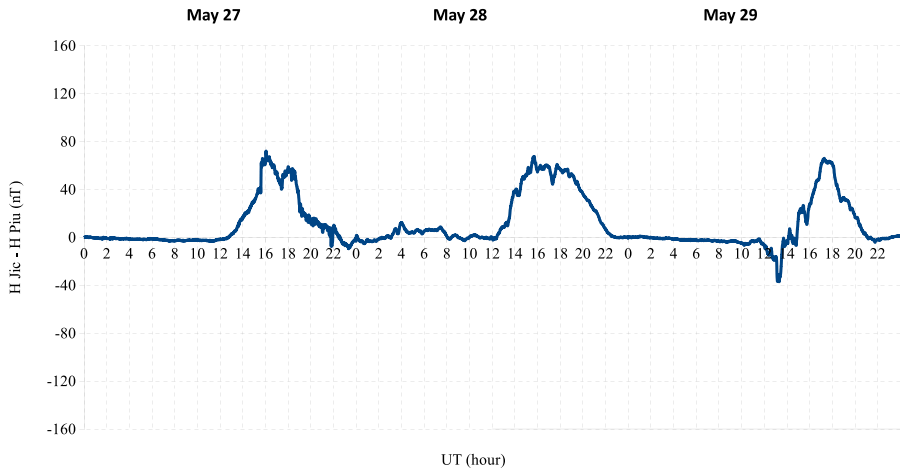


Fig. 15 Difference between horizontal geomagnetic field components (H) at Jicamarca and Piura, Peru, during 27–29 May 2017

create a latitudinal asymmetry in the EIA that may retard or suppress the development of the irregularities. It seems reasonable to suggest that the trans-equatorial/meridional winds might be one reason for the absence of irregularities during these periods.

In Tucumán, during the descending phase of solar cycle 24, the low spread-F occurrence season was equinox and the high spread-F season was summer except in 2018 when the highest spread-F occurrence was winter (González 2021). In this study, spread-F was absent during the storms of October 2015, March 2016 (equinox) and August 2018 (local winter), whereas it was present during the May 2017 storm (local winter). Becker-Guedes et al. (2004) showed that, in the Brazilian sector, geomagnetic storms trigger post-sunset spread-F during the low spread-F occurrence season and inhibit it during the high spread-F occurrence season. Our observations partially agree with this statement: irregularities did not develop during a storm occurred in a month of high spread-F occurrence rate (August 2018, local winter) over Tucumán.

5 Conclusions

We examined the occurrence of ionospheric irregularities during four geomagnetic storms (7/10/2015, 6/3/2016, 27/5/2017 and 25/8/2018) at a station near the southern crest of the EIA in South America (Tucumán, 26.9°S, 294.6°E, dip latitude 15.5°S).

The main outcomes of this study are:

1. RSF, moderate TEC fluctuation and weak GPS L band scintillation were seen during the main phase of the May storm, an intense storm driven by a CME. The irregularities onset was ~ 22 LT and lasted until post-midnight. We suggest that eastward DDEF and over-shielding electric fields may be responsible for the generation of these irregularities.

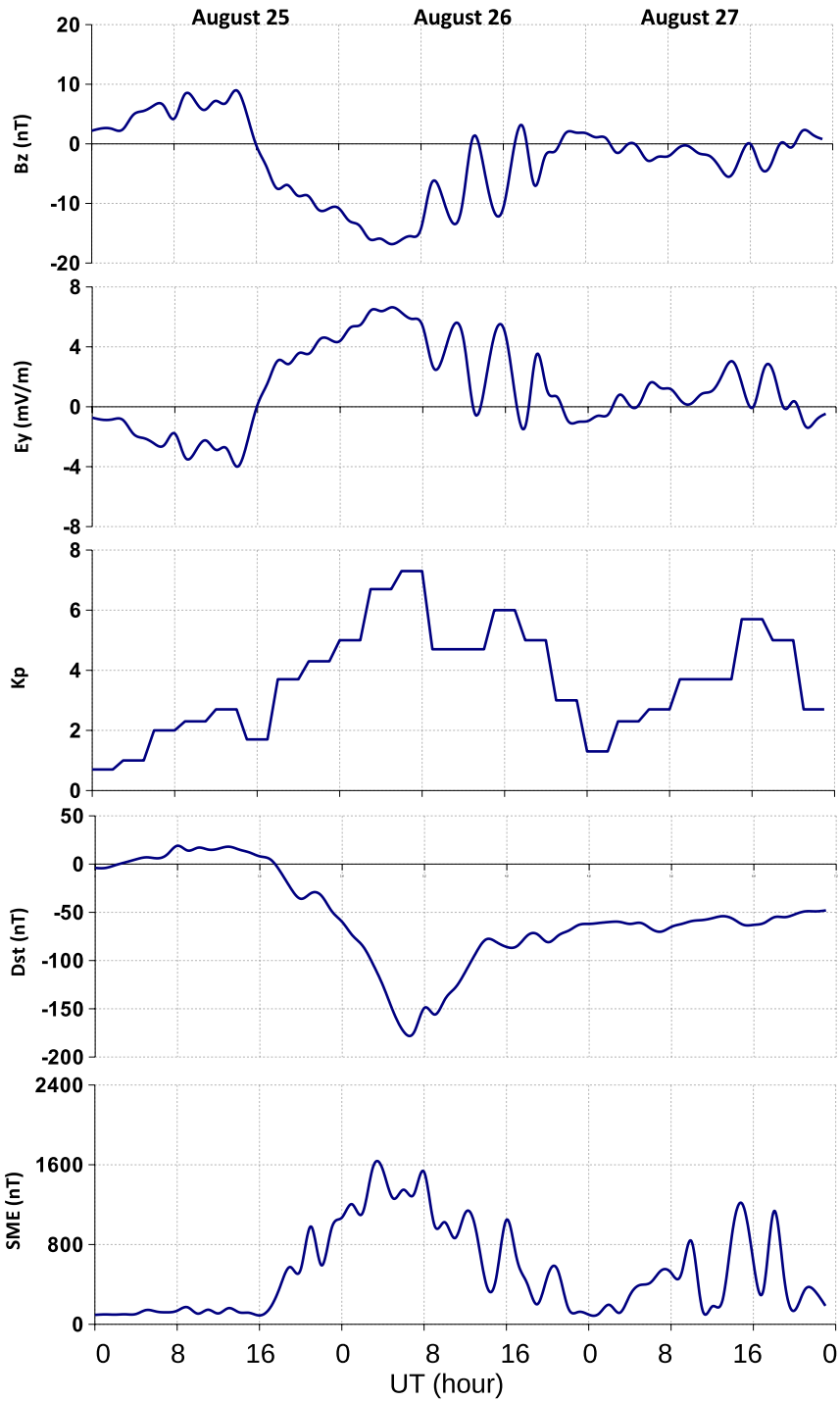


Fig. 16 B_z , E_y , K_p , Dst and SME during 25–27 August 2018

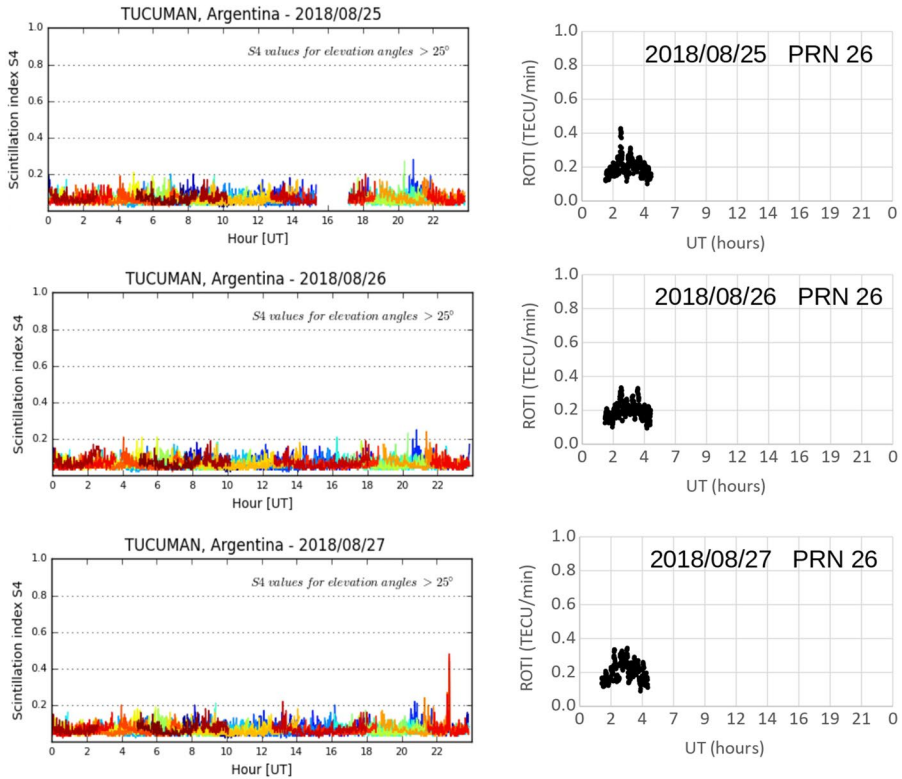


Fig. 17 S_4 index (left) at Tucumán during 25–27 August 2018. Different colours indicate different satellites. ROTI for PRN 26 (right) during 25–27 August 2018. (Color figure online)

2. Ionospheric irregularities were absent during the other three storms analysed. A possibility is that westward PPEFs and DDEFs may inhibit the growth of the irregularities.
3. Other factors might also affect the generation of irregularities during the considered storms. Some of them are the meridional disturbance winds, which may change the field line integrated conductivity of the unstable flux tubes and therefore influence the growth of an instability process, and TIDs due to storm time Joule heating. This needs to be further analysed.

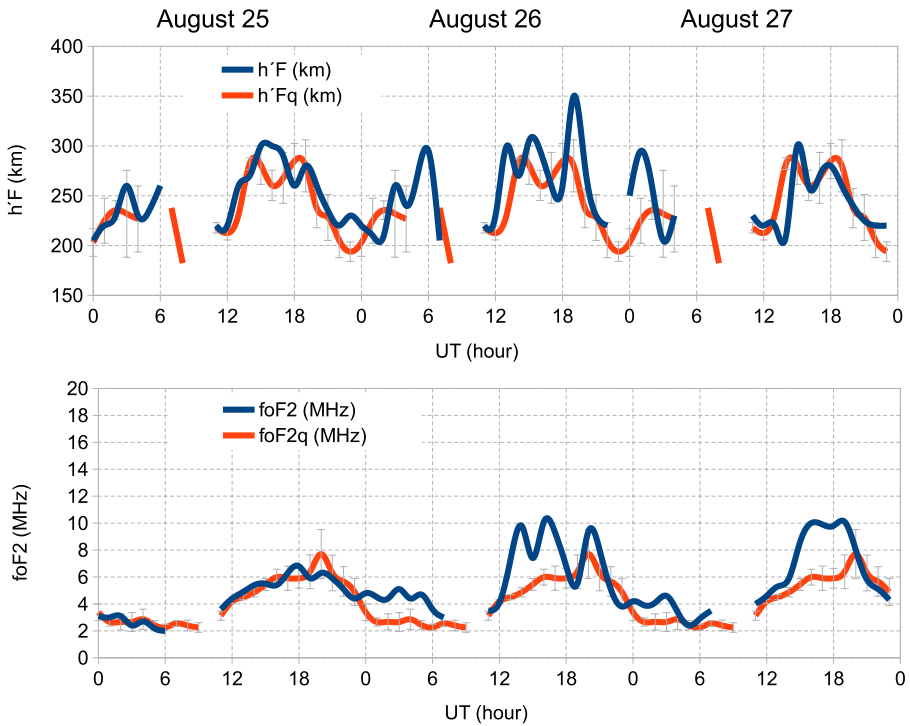


Fig. 18 $h'F$ (top) and $foF2$ (bottom) for Tucumán during 25–27 August 2018. The grey lines are ± 1 standard deviation of the average quiet day's value

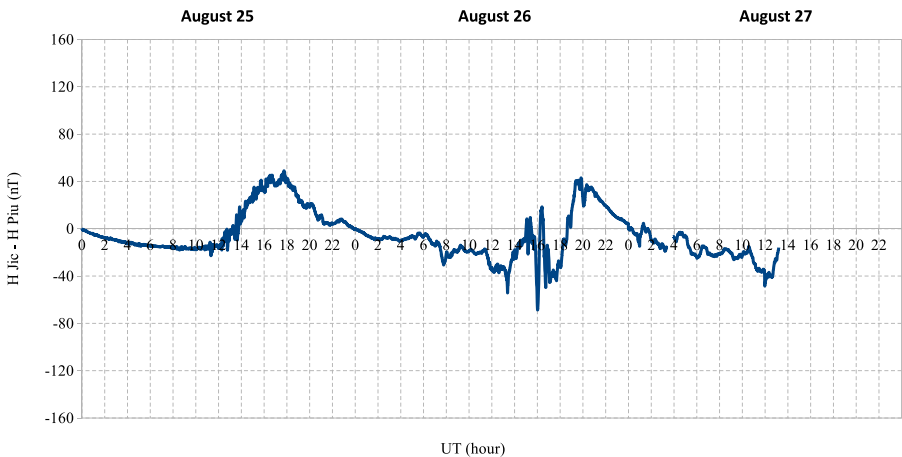


Fig. 19 Difference between horizontal geomagnetic field components (H) at Jicamarca and Piura, Peru, during 25–27 August 2018

Acknowledgements The Low Latitude Ionospheric Sensor Network (LISN) is funded by NSF Grant AGS-1933056 and is a project led by the University of Texas at Dallas in collaboration with the Geophysical Institute of Peru and other institutions that provide information in benefit of the space weather scientific community. We thank all organizations and persons that are supporting and operating VIPIR ionosondes

and GPS receivers under the LISN project. Thanks to the following groups for making data publicly available: the UMass Lowell Center for Atmospheric Research; the NASA/Goddard's Space Physics Data Facility; the International Service of Geomagnetic Indices; the GFZ German Research Center for Geosciences at Potsdam and the World Data Center (WDC) Kyoto, Japan. Thanks to Dr Victor H. Ríos for his helpful comments.

Funding The present study was supported by Universidad del Norte Santo Tomás de Aquino.

Declarations

Conflict of interest The author declares that she has no competing interest.

Data availability The ionosonde and GPS data are available at <http://lisn.igp.gob.pe/>

Code availability Not applicable.

References

- Aarons J (1991) The role of the ring current in the generation or inhibition of equatorial F layer irregularities during magnetic storms. *Radio Sci* 26(4):1131–1149. <https://doi.org/10.1029/91RS00473>
- Aarons J, Mullen JP, Koster JP, DaSilva RF, Medeiros JR, Medeiros RT, Paulson MR (1980) Seasonal and geomagnetic control of equatorial scintillations in two longitudinal sectors. *J Atmos Terr Phys* 42(9–10):861–866
- Abdu MA (1997) Major phenomena of the equatorial ionosphere-thermosphere system under disturbed conditions. *J Atmos Solar-Terr Phys* 59(13):1505–1519. [https://doi.org/10.1016/S1364-6826\(96\)00152-6](https://doi.org/10.1016/S1364-6826(96)00152-6)
- Abdu MA (2012) Equatorial spread F/plasma bubble irregularities under storm time disturbance electric fields. *J Atmos Solar Terr Phys* 75–76:44–56. <https://doi.org/10.1016/j.jastp.2011.04.024>
- Abdu MA, Brum CGM (2009) Electrodynamics of the vertical coupling processes in the atmosphere-ionosphere system of the low latitude region. *Earth Planets Space* 61(4):385–395. <https://doi.org/10.1186/BF03353156>
- Abdu MA, Batista PP, Batista IS, Brum CGM, Carrasco AJ, Reinisch BW (2006) Planetary wave oscillations in mesospheric winds, equatorial evening prereversal electric field and spread F. *Geophys Res Lett* 33(7):2–5. <https://doi.org/10.1029/2005GL024837>
- Abdu MA, Batista IS, Bertoni F, Reinisch BW, Kherani EA, Sobral JHA (2012) Equatorial ionosphere responses to two magnetic storms of moderate intensity from conjugate point observations in Brazil. *J Geophys Res Space Phys* 117(5):1–20. <https://doi.org/10.1029/2011JA017174>
- Alex S, Rastogi RG (1986) Geomagnetic disturbance effect on equatorial spread-F. *Ann Geophys* 2(2):82–88
- Astafyeva E, Zakharenkova I, Hozumi K, Alken P, Coïsson P, Hairston MR, Coley WR (2018) Study of the equatorial and low-latitude electrodynamic and ionospheric disturbances during the 22–23 June 2015 geomagnetic storm using ground-based and spaceborne techniques. *J Geophys Res Space Phys* 123(3):2424–2440. <https://doi.org/10.1002/2017JA024981>
- Balsley BB, Haerendel G, Greenwald RA (1972) Equatorial spread F: recent observations and a new interpretation. *J Geophys Res* 77(28):5625–5628. <https://doi.org/10.1029/JA077i028p05625>
- Basu S, MacKenzie E, Basu S (1988) Ionospheric constraints on VHF/UHF communications links during solar maximum and minimum periods. *Radio Sci* 23(3):363–378. <https://doi.org/10.1029/RS023i003p00363>
- Becker-Guedes F, Sahai Y, Fagundes PR, Lima WLC, Pillat VG, Abalde JR, Bittencourt JA (2004) Geomagnetic storm and equatorial spread-F. *Ann Geophys* 22(9):3231–3239. <https://doi.org/10.5194/angeo-22-3231-2004>
- Blanc M, Richmond AD (1980) The ionospheric dynamo. *J Geophys Res* 85(9):1669–1686. <https://doi.org/10.1029/JA085iA04p01669>
- Bolaji OS, Adebisi SJ, Fashae JB (2019) Characterization of ionospheric irregularities at different longitudes during quiet and disturbed geomagnetic conditions. *J Atmos Solar Terr Phys* 182:93–100. <https://doi.org/10.1016/j.jastp.2018.11.007>
- Borovsky JE, Denton MH (2006) Differences between CME-driven storms and CIR-driven storms. *J Geophys Res* 111(A7):A07S08. <https://doi.org/10.1029/2005JA011447>

- Briggs BH, Parkin IA (1963) On the variation of radio star and satellite scintillations with zenith angle. *J Atmos Terr Phys* 25(6):339–366. [https://doi.org/10.1016/0021-9169\(63\)90150-8](https://doi.org/10.1016/0021-9169(63)90150-8)
- Bullett T (2008) Station report : a new ionosonde at Boulder (issue November). https://www.sws.bom.gov.au/IPSHosted/INAG/web-69/2008/boulder_vipir.pdf
- Candido CMN, Batista IS, Becker-Guedes F, Abdu MA, Sobral JHA, Takahashi H (2011) Spread F occurrence over a southern anomaly crest location in Brazil during June solstice of solar minimum activity. *J Geophys Res Space Phys* 116(6):2008–2009. <https://doi.org/10.1029/2010JA016374>
- Dabas RS, Lakshmi DR, Reddy BM (1989) Effect of geomagnetic disturbances on the VHF nighttime scintillation activity at equatorial and low latitudes. *Radio Sci* 24(4):563–573. <https://doi.org/10.1029/RS024i004p00563>
- Dao T, Otsuka Y, Shiokawa K, Nishioka M, Yamamoto M, Buhari SM, Abdullah M, Husin A (2017) Coordinated observations of postmidnight irregularities and thermospheric neutral winds and temperatures at low latitudes. *J Geophys Res Space Phys* 122(7):7504–7518. <https://doi.org/10.1002/2017JA024048>
- Dashora N, Pandey R (2005) Observations in equatorial anomaly region of total electron content enhancements and depletions. *Ann Geophys* 23(7):2449–2456. <https://doi.org/10.5194/angeo-23-2449-2005>
- Davies K (1990). *Ionospheric Radio*. <https://doi.org/10.1049/pbew031e>
- Davis TN, Sugiura M (1966) Auroral electrojet activity index *AE* and its universal time variations. *J Geophys Res* 71(3):785–801. <https://doi.org/10.1029/JZ071i003p00785>
- de González GL (2021) Spread-F characteristics over Tucumán near the southern anomaly crest in South America during the descending phase of solar cycle 24. *Adv Space Res*. <https://doi.org/10.1016/j.asr.2021.11.009>
- de Abreu AJ, Martin IM, Fagundes PR, Venkatesh K, Batista IS, de Jesus R, Wild M (2017) Ionospheric F-region observations over American sector during an intense space weather event using multi-instruments. *J Atmos Solar Terr Phys* 156:1–14. <https://doi.org/10.1016/j.jastp.2017.02.009>
- de Paula ER, Kherani EA, Abdu MA, Batista IS, Sobral JHA, Kantor IJ, Takahashi H, de Rezende LFC, Muella MTAH, Rodrigues FS, Kintner PM, Ledvina BM, Mitchell C, Groves KM (2007) Characteristics of the ionospheric F-region plasma irregularities over Brazilian longitudinal sector. *Indian J Radio Space Phys* 36(4):268–277
- de Paula ER, de Oliveira CBA, Caton RG, Negreti PM, Batista IS, Martinon ARF, Moraes AO (2019) Ionospheric irregularity behavior during the September 6–10, 2017 magnetic storm over Brazilian equatorial–low latitudes. *Earth Planets Space*. <https://doi.org/10.1186/s40623-019-1020-z>
- De Siqueira Negreti PM, De Paula ER, Maria Nicoli Candido C (2017) Total electron content responses to HILDCAAs and geomagnetic storms over South America. *Ann Geophys* 35(6):1309–1326. <https://doi.org/10.5194/angeo-35-1309-2017>
- Deng Z, Wang R, Liu Y, Xu T, Wang Z, Chen G, Tang Q, Xu Z, Zhou C (2021) Investigation of low latitude spread-f triggered by nighttime medium-scale traveling ionospheric disturbance. *Remote Sens* 13(5):945. <https://doi.org/10.3390/rs13050945>
- Dugassa T, Habarulema JB, Nigussie M (2020) Statistical study of geomagnetic storm effects on the occurrence of ionospheric irregularities over equatorial/low-latitude region of Africa from 2001 to 2017. *J Atmos Solar Terr Phys* 199:105198. <https://doi.org/10.1016/j.jastp.2020.105198>
- Dungey JW (1956) Convective diffusion in the equatorial F region. *J Atmos Terr Phys* 9(5–6):304–310. [https://doi.org/10.1016/0021-9169\(56\)90148-9](https://doi.org/10.1016/0021-9169(56)90148-9)
- Fejer BG, Gonzales CA, Farley DT, Kelley MC, Woodman RF (1979) Equatorial electric fields during magnetically disturbed conditions—I. The effect of the interplanetary magnetic field. *J Geophys Res* 84(A10):5797–5802. <https://doi.org/10.1029/JA084iA10p05797>
- Fejer BG, Scherliess L, de Paula ER (1999) Effects of the vertical plasma drift velocity on the generation and evolution of equatorial spread F. *J Geophys Res Space Phys* 104(A9):19859–19869. <https://doi.org/10.1029/1999JA900271>
- Fejer BG, Jensen JW, Kikuchi T, Abdu MA, Chau JL (2007) Equatorial ionospheric electric fields during the November 2004 magnetic storm. *J Geophys Res Space Phys* 112(A10):10–15. <https://doi.org/10.1029/2007JA012376>
- Galav P, Sharma S, Pandey R (2011) Study of simultaneous penetration of electric fields and variation of total electron content in the day and night sectors during the geomagnetic storm of 23 May 2002. *J Geophys Res Space Phys* 116(12):1–10. <https://doi.org/10.1029/2011JA017002>
- Gonzalez WD, Tsurutani BT, Clúa De Gonzalez AL (1999) Interplanetary origin of geomagnetic storms. *Space Sci Rev* 88(3–4):529–562. <https://doi.org/10.1023/a:1005160129098>
- Huba JD, Krall J (2013) Impact of meridional winds on equatorial spread F: revisited. *Geophys Res Lett* 40(7):1268–1272. <https://doi.org/10.1002/grl.50292>
- Lyon AJ, Skinner NJ, Wright RWH (1960) The belt of equatorial spread-F. *J Atmos Terr Phys* 19(3–4):145–159. [https://doi.org/10.1016/0021-9169\(60\)90043-X](https://doi.org/10.1016/0021-9169(60)90043-X)

- Ma G, Maruyama T (2006) A super bubble detected by dense GPS network at east Asian longitudes. *Geophys Res Lett* 33(21):1–5. <https://doi.org/10.1029/2006GL027512>
- Madhav Haridas MK, Manju G, Arunamani T (2018) Solar activity variations of equatorial spread F occurrence and sustenance during different seasons over Indian longitudes: empirical model and causative mechanisms. *Adv Space Res* 61(10):2585–2592. <https://doi.org/10.1016/j.asr.2018.02.040>
- Magdaleno S, Herraiz M, de la Morena BA (2012) Characterization of equatorial plasma depletions detected from derived GPS data in South America. *J Atmos Solar Terr Phys* 74:136–144. <https://doi.org/10.1016/j.jastp.2011.10.014>
- Martinis CR, Mendillo MJ, Aarons J (2005) Toward a synthesis of equatorial spread F onset and suppression during geomagnetic storms. *J Geophys Res Space Phys* 110(A7):1–12. <https://doi.org/10.1029/2003JA010362>
- Maruyama T (1988) A diagnostic model for equatorial spread F, 1, Model description and application to electric field and neutral wind effects. *J Geophys Res* 93(A12):14611. <https://doi.org/10.1029/JA093iA12p14611>
- Maruyama T, Matuura N (1984) Longitudinal variability of annual changes in activity of equatorial spread F and plasma bubbles. *J Geophys Res* 89(A12):10903. <https://doi.org/10.1029/JA089iA12p10903>
- Matzka J, Stolle C, Yamazaki Y, Bronkalla O, Morschhauser A (2021) The geomagnetic Kp index and derived indices of geomagnetic activity. *Space Weather* 19(5):1–21. <https://doi.org/10.1029/2020SW002641>
- Nishioka M, Saito A, Tsugawa T (2008) Occurrence characteristics of plasma bubble derived from global ground-based GPS receiver networks. *J Geophys Res Space Phys* 113(5):1–12. <https://doi.org/10.1029/2007JA012605>
- Pi X, Mannucci AJ, Lindqwister UJ, Ho CM (1997) Monitoring of global ionospheric irregularities using the worldwide GPS network. *Geophys Res Lett* 24(18):2283–2286. <https://doi.org/10.1029/97GL02273>
- Piersanti M, De Michelis P, Del Moro D, Tozzi R, Pezzopane M, Consolini G, Diego P (2020) From the Sun to Earth: effects of the 25 August 2018 geomagnetic storm. *Ann Geophys* 38(3):703–724. <https://doi.org/10.5194/angeo-38-703-2020>
- Piggott WR, Rawer K (1978) Revision of chapters 1–4 U.R.S.I. handbook of ionogram interpretation and reduction. Report UAG-23A. Boulder, Colorado: World Data Center A for Solar-Terrestrial Physics, NOAA. https://www.sws.bom.gov.au/IPSHosted/INAG/uag_23a/uag_23a.html
- Ray S, Roy B, Das A (2015) Occurrence of equatorial spread F during intense geomagnetic storms. *Radio Sci* 50(7):563–573. <https://doi.org/10.1002/2014RS005422>
- Rishbeth H (1971) Polarization fields produced by winds in the equatorial F-region. *Planet Space Sci* 19(3):357–369. [https://doi.org/10.1016/0032-0633\(71\)90098-5](https://doi.org/10.1016/0032-0633(71)90098-5)
- Sahai Y, Becker-Guedes F, Fagundes PR, Lima WLC, Otsuka Y, Huang CS, Bittencourt JA (2007) Response of nighttime equatorial and low latitude F-region to the geomagnetic storm of August 18, 2003, in the Brazilian sector. *Adv Space Res* 39(8):1325–1334. <https://doi.org/10.1016/j.asr.2007.02.064>
- Sahai Y, Fagundes PR, de Jesus R, de Abreu AJ, Crowley G, Kikuchi T, Bittencourt JA (2011) Studies of ionospheric F-region response in the Latin American sector during the geomagnetic storm of 21–22 January 2005. *Ann Geophys* 29(5):919–929. <https://doi.org/10.5194/angeo-29-919-2011>
- Seemala GK, Valladares CE (2011) Statistics of total electron content depletions observed over the South American continent for the year 2008. *Radio Sci* 46(5):1–14. <https://doi.org/10.1029/2011RS004722>
- Senior C, Blanc M (1984) On the control of magnetospheric convection by the spatial distribution of ionospheric conductivities. *J Geophys Res* 89(A1):261–284. <https://doi.org/10.1029/JA089iA01p00261>
- Shang SP, Shi JK, Kintner PM, Zhen WM, Luo XG, Wu SZ, Wang GJ (2008) Response of Hainan GPS ionospheric scintillations to the different strong magnetic storm conditions. *Adv Space Res* 41(4):579–586. <https://doi.org/10.1016/j.asr.2007.05.020>
- Singh R, Sripathi S, Sreekumar S, Banola S, Emperumal K, Tiwari P, Kumar BS (2015) Low-latitude ionosphere response to super geomagnetic storm of 17/18 March 2015: results from a chain of ground-based observations over Indian sector. *J Geophys Res Space Physics* 120(12):10864–10882. <https://doi.org/10.1002/2015JA021509>
- Tsunoda RT (2006) Day-to-day variability in equatorial spread F: is there some physics missing? *Geophys Res Lett* 33(16):15. <https://doi.org/10.1029/2006GL025956>
- Valladares CE, Villalobos J, Sheehan R, Hagan MP (2004) Latitudinal extension of low-latitude scintillations measured with a network of GPS receivers. *Ann Geophys* 22(9):3155–3175. <https://doi.org/10.5194/angeo-22-3155-2004>

- Wei Y, Fraenz M, Dubinin E, He M, Ren Z, Zhao B, Alex S (2013) Can a nightside geomagnetic Delta H observed at the equator manifest a penetration electric field? *J Geophys Res Space Phys* 118(6):3557–3567. <https://doi.org/10.1002/jgra.50174>
- Wei Y, Zhao B, Li G, Wan W (2015) Electric field penetration into Earth's ionosphere: a brief review for 2000–2013. *Sci Bull* 60(8):748–761. <https://doi.org/10.1007/s11434-015-0749-4>